J Mater Sci (2011) 46:215–227
DOI 10.1007/s10853-010-4928-z

The influence of biaxial strain ratio and strain range on crack growth mode and crack shape

T. H. Topper · J. J. F. Bonnen · M. Khalil · A. Varvani-Farahani

Received: 24 October 2009 / Accepted: 14 September 2010 / Published online: 2 October 2010

Abstract Axial-torsion tests were used to determine and model the combinations of strain range and crack length at which the crack growth changed from a shear to a tensile mode. Biaxial tests and confocal scanning laser microscopy (CSLM) were used to observe crack shape evolution at various strain ratios. Constant and variable amplitude loading of notched specimens and CSLM were used to determine the dependence of crack shape development on strain range. The results showed that, except for very high strain levels, at strain ratios causing shear mode crack growth multiple cracks initiated and grew until they were semicircular and then linked up to cause failure. For tensile mode crack growth at low strains a single crack grew into and maintained a semicircular shape. At high strain ranges multiple cracks formed and linked up to maintain an elongated crack shape.

T. H. Topper
Department of Civil and Environmental Engineering, University of Waterloo, Waterloo, ON, Canada
e-mail: topper@uwaterloo.ca

J. J. F. Bonnen (✉)
Manufacturing Research Department, Ford Research and Innovation Center, Dearborn, MI, USA
e-mail: john.bonnen@gmail.com

M. Khalil
Bombardier, Toronto, ON, Canada
e-mail: mohamed.khalil1@gmail.com

A. Varvani-Farahani
Department of Mechanical & Industrial Engineering, Ryerson University, Toronto, ON, Canada
e-mail: avarvani@ryerson.ca

Introduction

This article examines the effect of crack closure biaxial strain ratio and the magnitude of cyclic straining on fatigue crack initiation and early crack growth. A number of investigators [1–4] have shown that reductions in crack closure in mode I crack growth or in the equivalent crack face interference in other modes due to overloads can drastically change the growth rate of small cracks and reduce fatigue resistance, but there is little information on whether there is a corresponding change in cracking mode or crack shape development. Of particular interest is whether the changeover from mode II to mode I crack growth, which usually occurs at a very short crack length when a significant amount of crack face interference is present, would also take place in crack closure-free crack growth. The reason for the interest in crack face interference-free small crack growth is that the high local strain levels that are present when small cracks grow from notches under service fatigue loads introduce large reductions in crack face interference. Two theories concerning the mode in which a fatigue crack will grow [5] are compared with experimental data in a later section of this article.

Cracking mode and crack shape development depend on both biaxial strain ratio and the magnitude of the cyclic strains as well as the amount of crack face interference. Brown and Miller [6] and Socie [7] have provided comprehensive reviews of the literature on crack initiation and crack growth planes under biaxial loading. Methods of measuring the surface crack length of small cracks have included optical and scanning electron microscopy of specimen surfaces. In the past 15 years confocal scanning laser microscopy (CSLM) has provided an accurate method of measuring the size and shape of small cracks growing into a surface [8]. The system we use [8] has a resolution of

0.25 and 0.50 μm in measuring the length and depth of a crack, respectively.

In uniaxial fatigue Newman and Edwards [9] reported that for strains for smooth specimens near the fatigue limit, a single crack usually grew to failure. It started as a shallow surface crack changed in shape until it became semicircular and then retained that shape until failure. On the other hand at high strains many cracks typically linked together to form a dominant crack with an elongated shape.

In this article we review investigations [1, 5, 10] in which crack growth mode and crack shape development were monitored for various positive and negative strain ratios at relatively low strains in thin-walled tubes subjected to internal and external pressure and axial load. Fully reversed straining histories and straining histories containing compressive overloads normal to the crack face that eliminated crack face interference were used. These tests were supplemented by uniaxial tests of notched specimens in which crack shape development was monitored for notched specimens under constant amplitude and a standard SAE service load history for various strain levels [12].

Also reported is an investigation in which mode II crack growth data obtained from a slit tubular specimen tested in a tension-torsion fatigue machine under a special load history that eliminated crack face interference was used together with closure-free mode I crack growth data to evaluate two theories predicting the changeover from mode II to mode I crack growth for various tension torsion strain ratios [5]. The predictions are compared to observed changeovers in tension-torsion tests, and fatigue life predictions using the theories are compared to fatigue test results.

Changes of crack growth mode and crack shape development with strain ratio

Biaxial fatigue tests were performed under internal and external pressure and axial load on thin-walled tubular specimens of as received SAE 1045 steel while uniaxial tests were performed on round dogbone specimens with a flat region in the gage length. The specimens are shown in Fig. 1, and the biaxial fatigue machine is described in Ref. [10]. Biaxial strain ratios (ratio of hoop strain to axial strain $\lambda = \varepsilon_h/\varepsilon_a$ or second to first principal strains, $\lambda = \varepsilon_{22}/\varepsilon_{11}$) of $\lambda = -1$ and $\lambda = -0.625$ (shear straining), $\lambda = -v$ (uniaxial straining), and $\lambda = +1$ (equibiaxial straining) were used. The biaxial load histories employed are shown in Fig. 2 with the constant amplitude histories on the left and the compressive overload histories on the right in each figure. The number of small cycles in the overload histories was chosen so that the overstrain fatigue damage was about 20% of the total fatigue damage.

Crack opening stress, crack depth, and crack shape measurements

To measure crack geometries and check crack opening stresses, tests were stopped and specimens were taken out of the test machines and transported to the CSLM. Smooth uniaxial specimens were mounted in a tensometer. The specimen and tensometer were mounted in a goniometer holder and placed under the laser microscope. The specimen was tilted to adjust the angle to give the greatest crack depth as the specimen was tensioned until the stress reached the same maximum stress as the last fatigue cycle applied. Images from different crack depths were obtained at increasing stress levels by changing the specimen height using a piezo-electric monitored stage. A set of confocal image slices were obtained at depth steps of 3 μm. Post image processing was used to obtain the three dimensional geometry of the crack at each stress level. The crack opening stress (the stress at which the crack first reached its maximum depth) and the final crack geometry were recorded. The procedure for measuring crack geometries and obtaining crack opening stresses in smooth tubular specimens was the same as for the uniaxial specimens except that the crack was opened by capping the specimen and applying internal pressure via oil pressurized by a

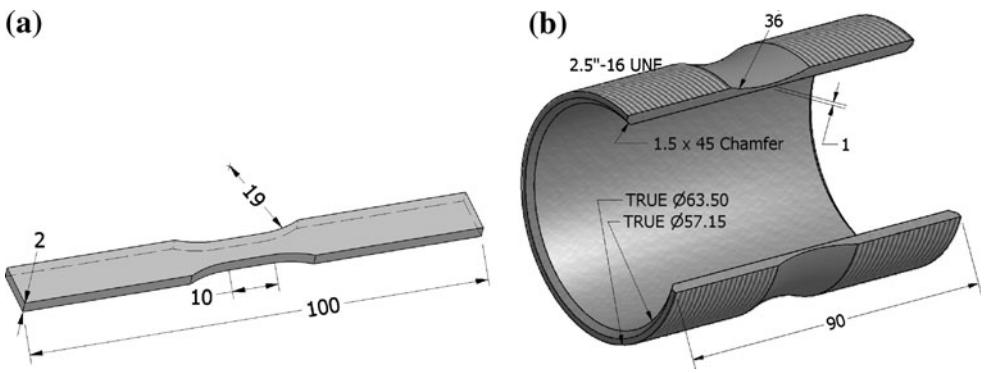

Fig. 1 **a** Flat uniaxial dogbone specimen, and **b** biaxial (axial—internal/external pressure) tubular specimen

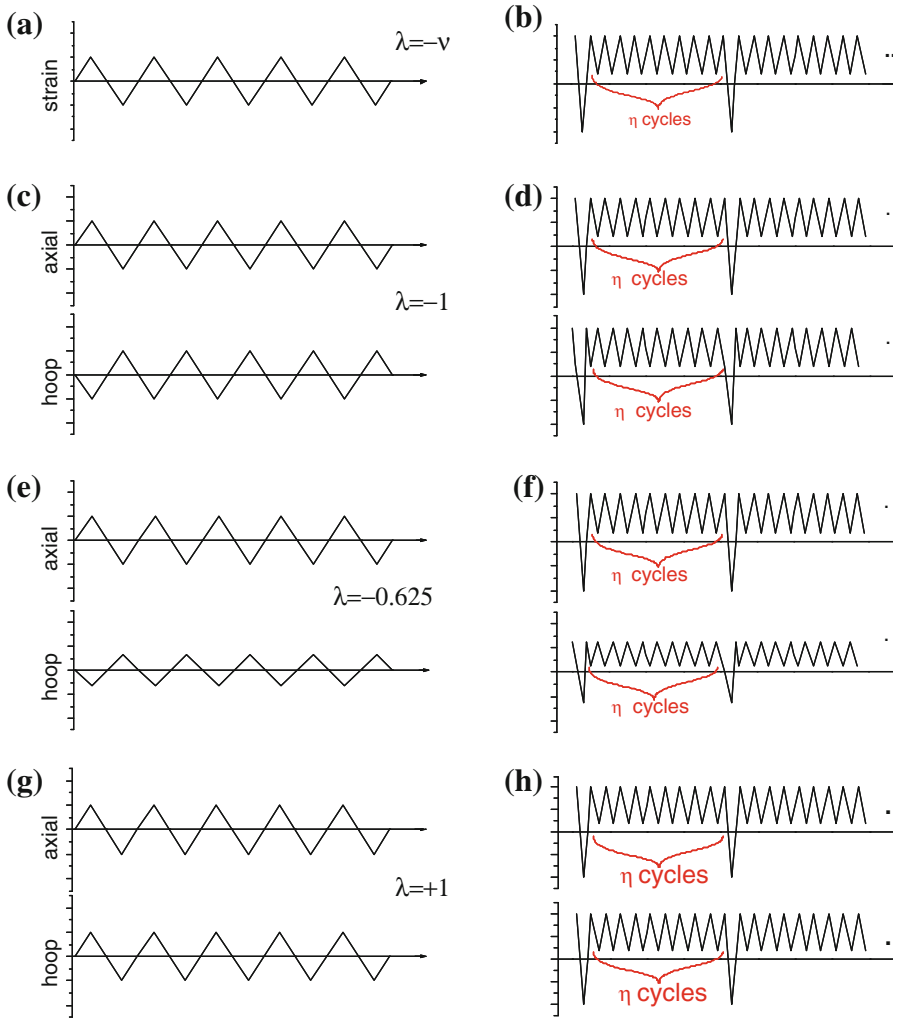

Fig. 2 Typical constant amplitude (**a**, **c**, **e**, **g**) and periodic compressive overload strain histories (**b**, **d**, **f**, **h**) applied to the specimens shown in Fig. 1. Uniaxial or $\lambda = -\nu$ (**a**, **b**), pure shear or $\lambda = -1$ (**c**, **d**), $\lambda = -0.625$ (**e**, **f**), and equibiaxial histories [$\lambda = +1$ (**g**, **h**)] are shown [2]

small hand pump to pressures measured by a pressure gage that corresponded to desired stress levels. Figure 3 shows the optical sectioning of a small crack and gives the cross section at a point L_i from the left-hand end of a fully open crack. The depth of the crack was taken as the average of the peaks at the crack mouth. Figure 4 shows a plot of crack front measurements for two $\lambda = -1$ cracks, cracks 1 and 2 and an equibiaxial crack, crack 3.

Crack shape evolution in constant amplitude straining

In both constant amplitude and overload tests under uniaxial and equibiaxial straining cracks initiated and grew through one or two grains on the maximum shear planes at 45° to the specimen surface. Then the cracks rotated and continued in mode I growth normal to the axis of straining. In uniaxial straining the cracks grew on the single plane of maximum shear whereas in equibiaxial straining they grew on the two maximum shear planes parallel and perpendicular to the specimen axis. The pattern of crack shape evolution was the same for the two strain ratios and for constant amplitude and overload tests. The cracks were initially long and shallow ($a/c = 0.2$) but grew more rapidly in the depth than the length direction until they reached a depth a to half length c ratio of 0.8 after which they continued to maintain this shape. Figure 5 shows the initial changes of aspect ratio with crack depth for a variety of equibiaxial strain amplitudes. Since the values of a/c fall on a single curve and a given crack depth corresponds closely to the same fatigue life fraction at all strain amplitudes this implies that crack shape will be the same at a given fatigue life fraction for all strain amplitudes.

The pattern of crack shape evolution in $\lambda = -1$ and $\lambda = -0.625$ straining was the same for the two strain ratios and for both constant amplitude and overload strain histories. Many microcracks initiated and grew into the specimens. The number of microcracks increased as a test progressed, but for most of the fatigue life their surface length did not increase much. During this time the cracks

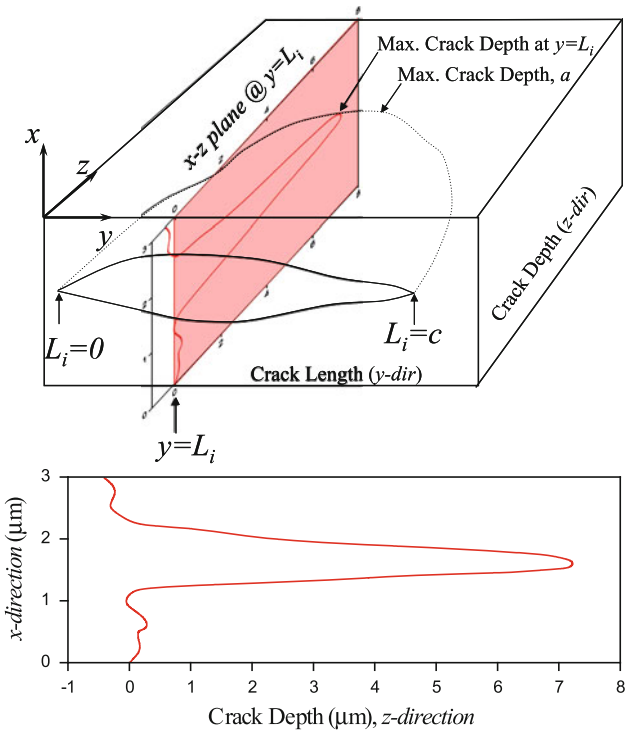

Fig. 3 Optical section obtained from the 3-d crack using a goniometer and a confocal scanning laser microscope [11]

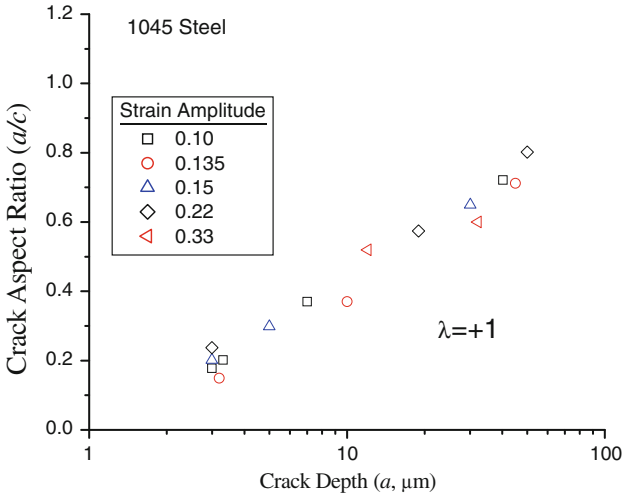

Fig. 5 Crack aspect ratio versus the crack depth for equibiaxial loading, $\lambda = +1$ [2]

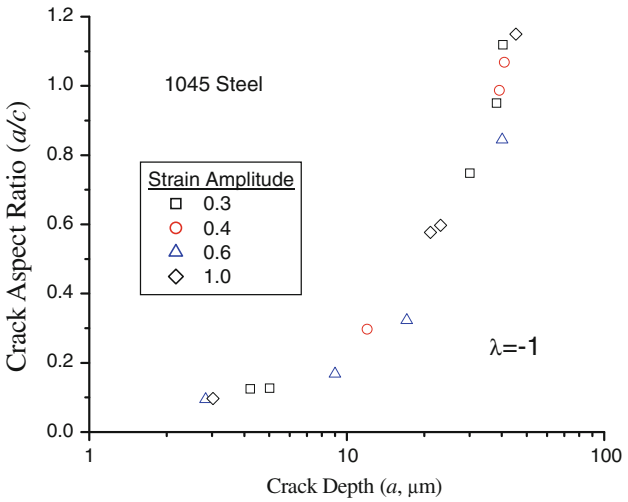

Fig. 6 Crack aspect ratio versus the crack depth for shear loading, $\lambda = -1$ [2]

grew into the specimen and their shape changed from a long shallow ellipse to an ellipse with a depth slightly exceeding its half length. Figure 6 gives a plot of the changes in aspect ratio with crack depth for pure shear straining at various strain amplitudes. The values of *a*/*c* with crack depth fall on a single curve for all strain amplitudes indicating that the crack shape for all strain amplitudes is approximately the same at a given fatigue life fraction. When the cracks reached a value of *a*/*c* a little greater than 1 at a fatigue life fraction of 90–95% they started to grow in length as well as in depth and rapidly linked up on shear planes to form a crack 2–5 mm in length.

Figure 7 gives a schematic illustration of the evolution of crack shape in shear and equibiaxial straining. In pure shear (and in $\lambda = -0.625$ straining) the initiation and growth of cracks on planes of maximum shear occupied about 90% of the fatigue life. During this time the aspect ratio *a*/*c* increased until it exceeded 1. Then there was a rapid linking up of the cracks and failure. In equibiaxial (and uniaxial) straining on the other hand the aspect ratio of cracks increased to about 0.8 and then this shape was maintained as the crack grew in length and depth to failure.

Fig. 4 Crack front profiles for two $\lambda = -1$ cracks and one equibiaxial crack [2]

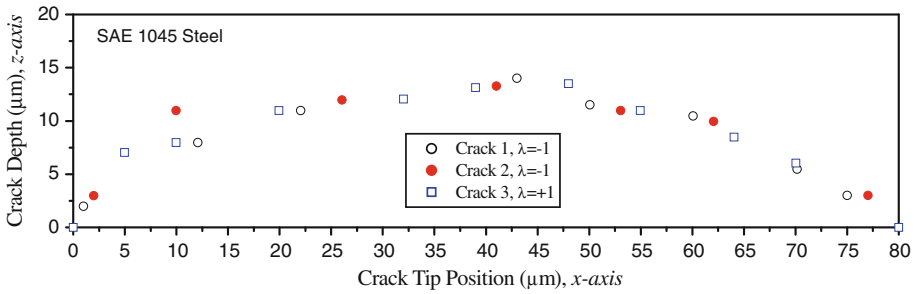

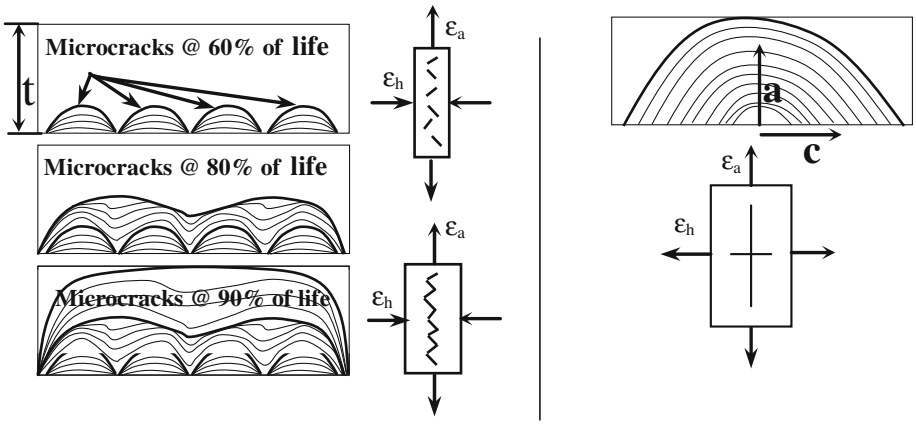

Fig. 7 Crack growth mechanisms for through thickness growth (t) for **a** shear ($\lambda = -1$) and **b** equibiaxial ($\lambda = +1$) loading [2]

Effect of periodic compressive overloads on crack growth

Although compressive overloads did not affect crack shape evolution significantly, they drastically accelerated crack growth rates and reduced fatigue life. Varvani-Farahani and Topper [10] showed that the compressive overloads reduced the height of asperities in the crack wake, and, once the overload stress approached the yield stress, cracks at all strain ratios were open at zero load. In the overload load histories used in the tests described here, the overloads were large enough that there was no crack face interference and the entire applied stress intensity was effective. Figure 8 gives shear strain versus equivalent fatigue life curves for the various strain ratios for constant amplitude tests and for tests with overload strains of 0.38% where the equivalent life is the life calculated after removing the damage due to the overload cycles in the overload tests. The overloads drastically reduced the lives with the reduction becoming greater as life increased. Figure 9 gives a plot of crack growth rate versus effective strain intensity range for mode I uniaxial and equibiaxial crack growth and mode III shear crack growth where the strain intensities were calculated for a semi-elliptical small crack using the strain intensity given in Ref. [13]. For the crack face interference-free conditions of these tests, crack growth rate versus effective strain intensity curves are about the same for the two crack growth modes.

The effect of strain range and strain history on crack shape

Although at the strain levels used in the thin tube specimens a single mode I crack grew to failure without linking up in uniaxial and equibiaxial tests it has been observed that at high strain ranges multiple mode I cracks develop and link up. The notched specimens shown in Fig. 10 were tested at various levels of constant amplitude strain and at various scaling levels of the standard SAE Grapple Skidder Torque load history [14] shown in Fig. 11. The reason for using a notched specimen is that crack initiation typically initiates at stress raisers. The reason for the use of different specimen radii was to determine whether cracks confined to the smaller region of maximum strain in the smaller radius notch would link up quicker than in the larger notch in which a larger region of maximum strain could lead to more cracks at different heights that would overlap without linking up. The material in these tests was quenched and tempered SAE 1045 steel with a Rockwell C hardness of 48. Crack geometry was monitored during the tests using the confocal scanning microscope techniques described in the previous section.

Constant amplitude tests

Three different fully reversed load amplitudes were applied to specimens of each of the two geometries. The lowest load level was chosen to give a notch root strain amplitude of 0.34% a level just above the metal's fatigue limit, the second load level was chosen to give a 0.51% local strain amplitude—1.5 times the fatigue limit, and the third load level was chosen to give a 0.68% local strain amplitude—twice the fatigue limit.

At the lowest load level only one crack was initiated in the 1.0- and the 5.0-mm notch radius specimens. The initially shallow shear cracks changed to mode I tensile cracks after growing through one or two grains. Then they grew more rapidly in depth than in length until they reached an aspect ratio of 0.9. They continued to grow at this aspect ratio until they reached the edges of the specimen after which they grew to failure as through cracks. The crack shape in the 5-mm notch at 23% of the fatigue life is shown in Fig. 12. At the small size of this crack, the influence of grain boundaries is believed to be evident.

At a strain amplitude of twice the fatigue limit (0.68%) multiple cracks initiated at numerous locations in the notch

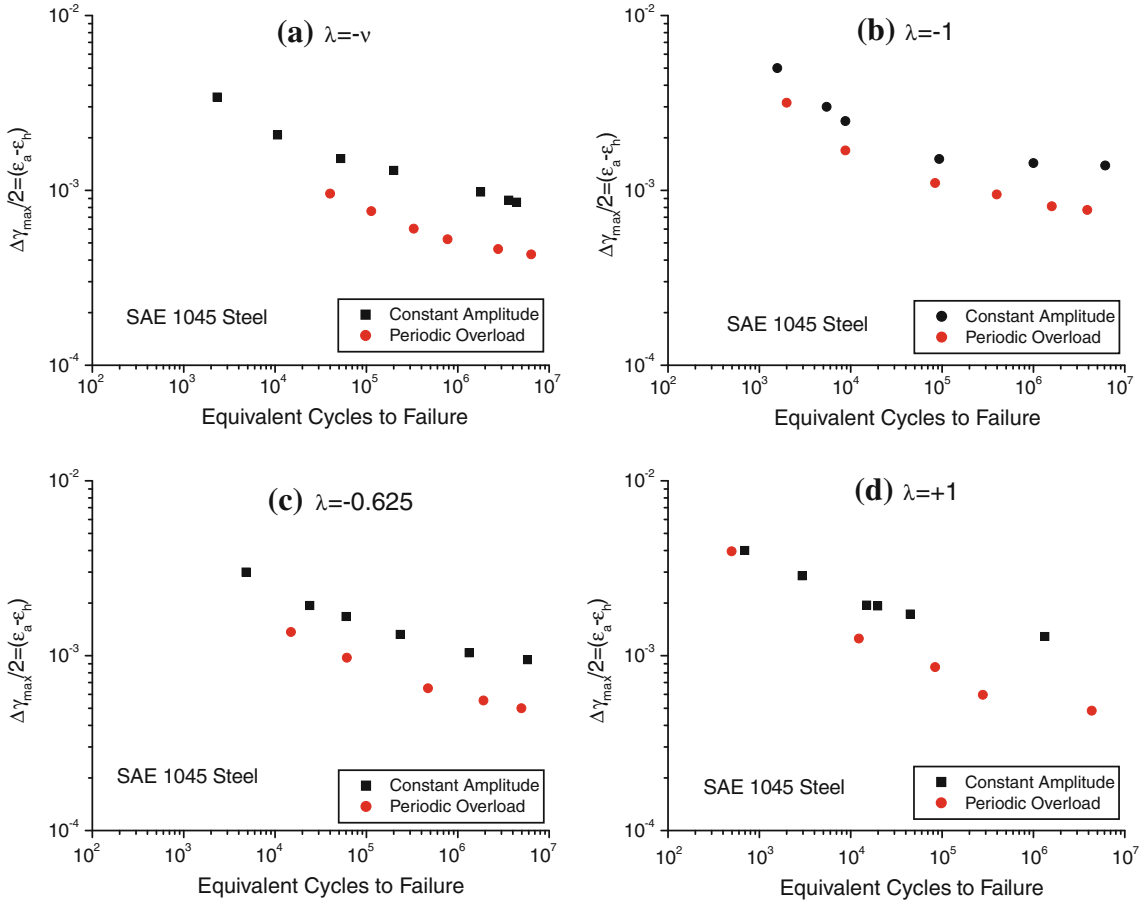

Fig. 8 Fatigue life data versus maximum shear strain component for constant amplitude and periodic compressive overload histories: **a** uniaxial straining ($\lambda = -\nu$), **b** shear straining ($\lambda = -1$), **c** biaxial straining at $\lambda = -0.625$, and **d** equibiaxial straining, $\lambda = +1$ [2]

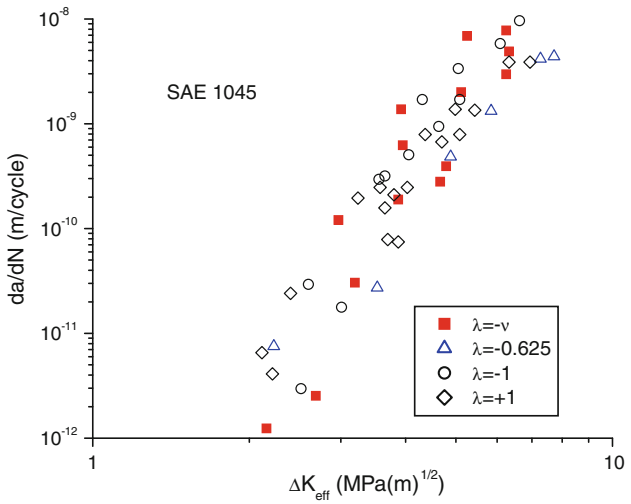

Fig. 9 Crack growth rates for various strain ratios plotted against effective strain intensity factor for in-phase periodic overload tests [2]

roots of both 1.0- and 5.0-mm specimens. After growing in a shear mode through the first few grains the cracks continued as mode I tensile cracks. An initial increase in aspect ratio was quickly followed by a decrease as the cracks linked up often after overlapping. During subsequent growth the cracks maintained an average aspect ratio of about 0.2 until they reached the edge of the specimen and became through cracks. Although there was somewhat less overlapping of cracks before they joined up in the 1.0-mm notch than in the 5.0-mm notch the stable values of the aspect ratios were about the same for the two notches.

At the intermediate strain amplitude of 0.51% many cracks initiated in both 1.0- and 5.0-mm notch roots and grew first in a shear mode through a few grains and changed to mode I. At first they grew more rapidly in depth than in length and their aspect ratio increased. When they grew enough in length they linked up often after overlapping to form several long cracks in the notch root. Continuous linking up of cracks maintained an average crack aspect ratio of about 0.5. Again although there was less overlapping of cracks in the 1.0- than in the 5.0-mm notches there was no noticeable difference in their average aspect ratios after cracks started linking up. The average aspect ratio continued to be about 0.5 until a crack

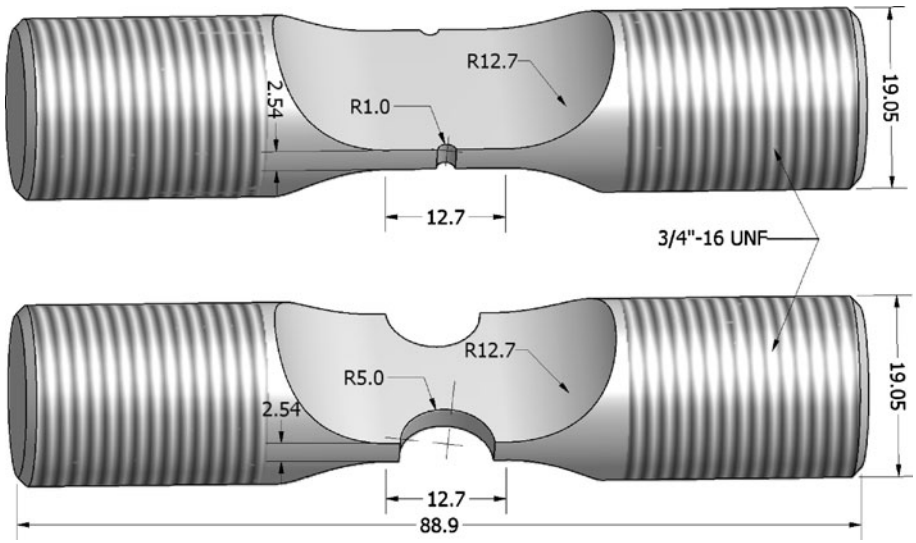

Fig. 10 Notched specimen designs used in constant amplitude and Grapple Skidder torque history testing. All dimensions in mm (with one exception noted)

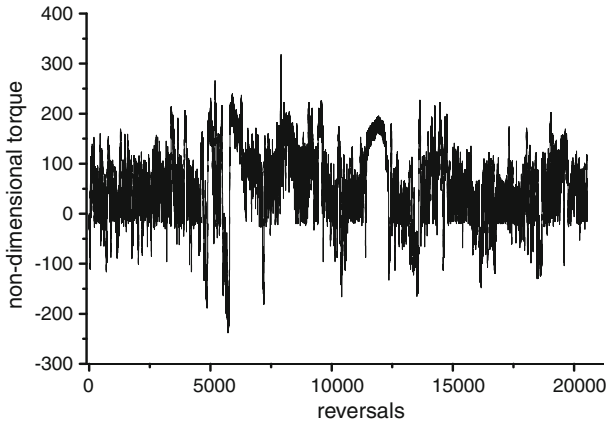

Fig. 11 Grapple Skidder torque history

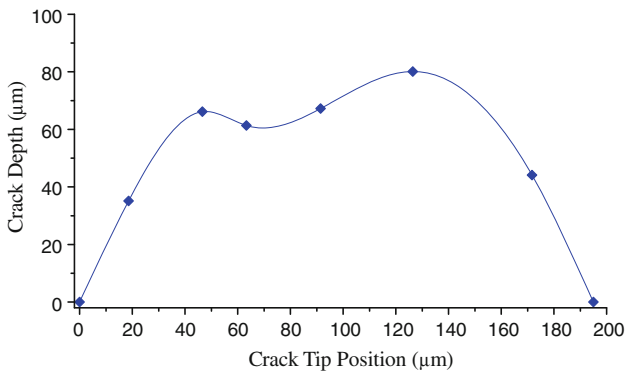

Fig. 12 Crack front profile under constant amplitude fatigue near the fatigue limit in a 5-mm notch

reached the edge of the specimen and became a through crack.

Figure 13 gives schematic diagrams for cracks propagating at the three different strain amplitudes showing the crack shape development. As the strain amplitude increases an increasingly rapid linking up of cracks lowers the stable value of the crack aspect ratio. Figure 14 gives a plot of aspect ratio versus strain amplitude data for the two notch sizes. There is no significant difference between the data for the two notch radii.

Crack shape evolution under the spectrum loading

The SAE Grapple Skidder load history was scaled to three levels that gave maximum local notch strain amplitudes of 0.42, 0.61, and 0.73% and applied to the 5.0-mm notched specimen. The pattern of the evolution of crack shape in these tests was similar to that in constant amplitude loading. For the load history having the lowest loads only one crack propagated. As in the lowest load level constant amplitude test, an initially shallow crack first increased its aspect ratio to a stable level (0.88) and then maintained this aspect ratio until the crack became a through crack on reaching the edges of the specimen.

Again as in the constant amplitude tests, multiple cracks initiated during the two higher spectrum load tests. After initially increasing their aspect ratio by growing faster in depth than in length, faster growth in the length direction led to a continuous linking up of cracks that maintained a stable aspect ratio. The aspect ratios were 0.36 and 0.17 for maximum strain levels of 0.61 and 0.73, respectively. Figure 15 gives a plot of aspect ratio versus maximum notch strain amplitude for these tests showing that as the strain amplitude increases the increasingly rapid linking up of cracks decreases the average crack aspect ratio.

Khalil [12] who performed similar tests on a 2024 T351 aluminum alloy observed the same trends in crack shape development with strain level under constant amplitude

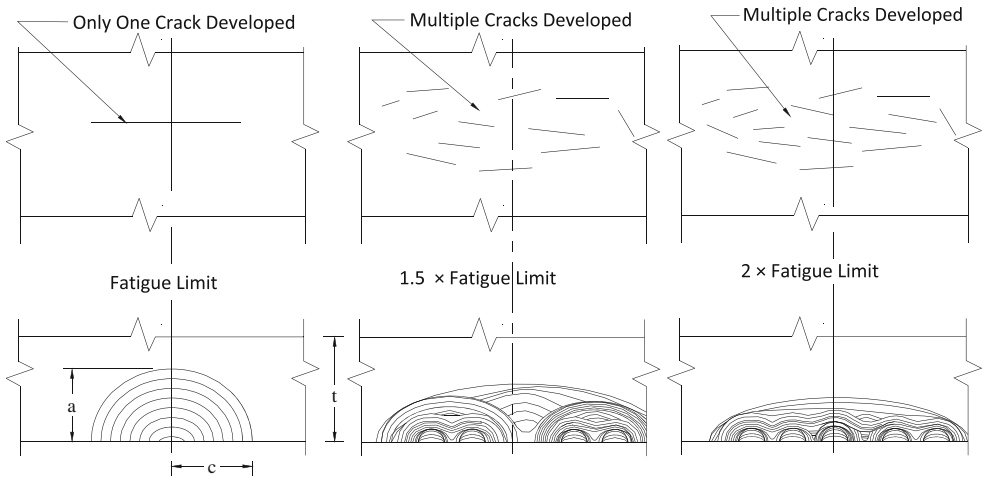

Fig. 13 Schematic diagram of crack linking at and above the fatigue limit

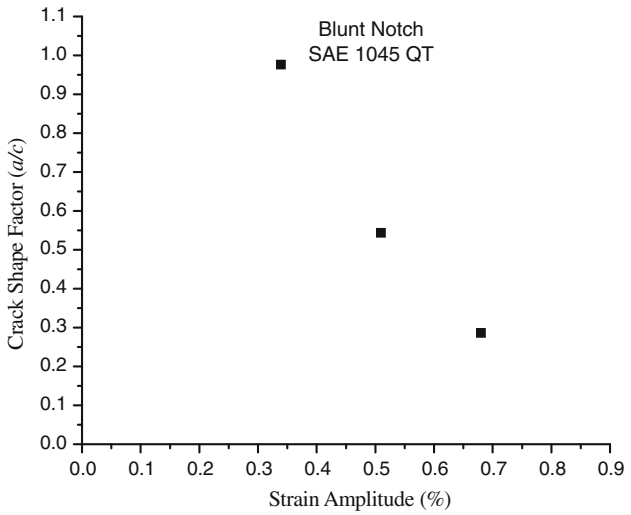

Fig. 14 Crack shape factor versus strain amplitude for constant amplitude fatigue of blunt (5 mm)-notched specimens in a 1045 QT steel

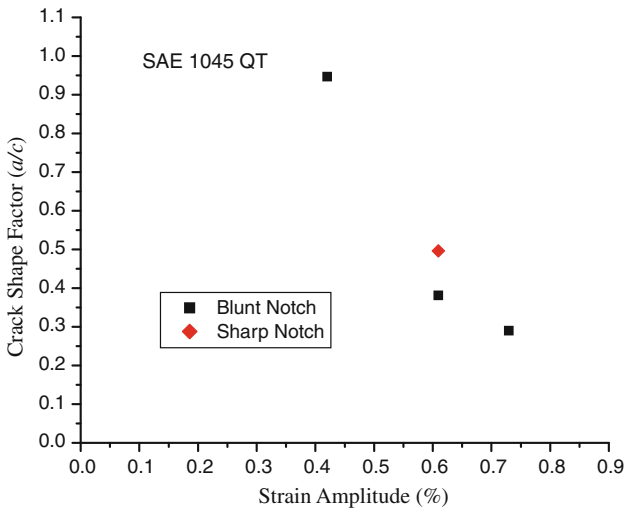

Fig. 15 Crack shape factor versus maximum strain amplitude of the Grapple Skidder torsion history for blunt- and sharp-notched specimens

and spectrum load histories in specimens having the same geometry.

Changes in cracking mode in crack face interference-free crack growth

As pointed out in the introduction there is an interest in crack face interference-free small crack growth because the high local strain levels that occur in notches during overloads in service load histories greatly reduce the amount of crack face interference in small cracks growing from the notch. The conditions for a change in crack growth mode under crack face interference-free conditions are expected to be similar to the conditions required for a mode change during service loading. Two theories that predict the mode in which a fatigue crack will grow have been advanced in Refs. [15, 16]. In the former, Nuismer suggests that a crack will grow in the mode in which the strain energy release rate is the greatest. In the latter, Hourlier and Pineau observed that cracks grew in the mode for which the crack growth rates were highest. Bonnen and Topper [5] applied these criteria to predict the length at which cracks would change from mode II to mode I growth as a function of strain ratio and strain range in crack face interference-free biaxial fatigue. In order to make the predictions they needed crack growth data for crack face interference-free crack growth in modes I, II, and III to insert into their strain-based short-crack growth model [5]. Data for modes I and III were available but because it has been difficult to

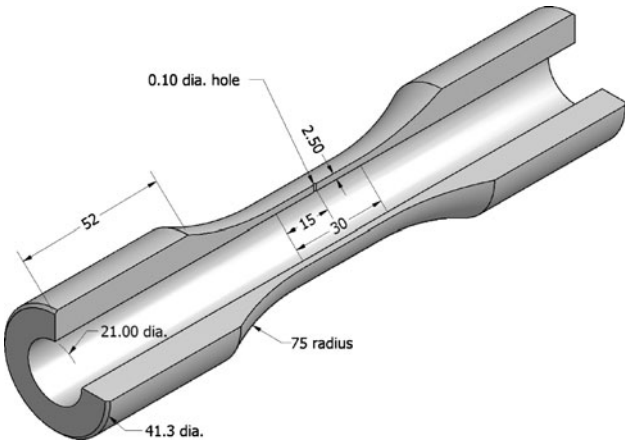

Fig. 16 Notched tubular mode II crack growth specimen. All dimensions in mm [5]

find conditions for which cracks will continue to grow in pure mode II they needed to generate the data. They believed that the reason that cracks did not grow in mode II in the usual constant amplitude tests was that there is a rapid buildup in crack face interference due to asperities in the crack wake such as those reported by Varvani-Farahani and Topper [10]. In order to grow cracks in mode II without crack face interference, Bonnen and Topper [5] used the specimen shown in Fig. 16 together with the special torsion load history shown in the inset in Fig. 17 in a torsion fatigue test. The torsion overload cycles shown in

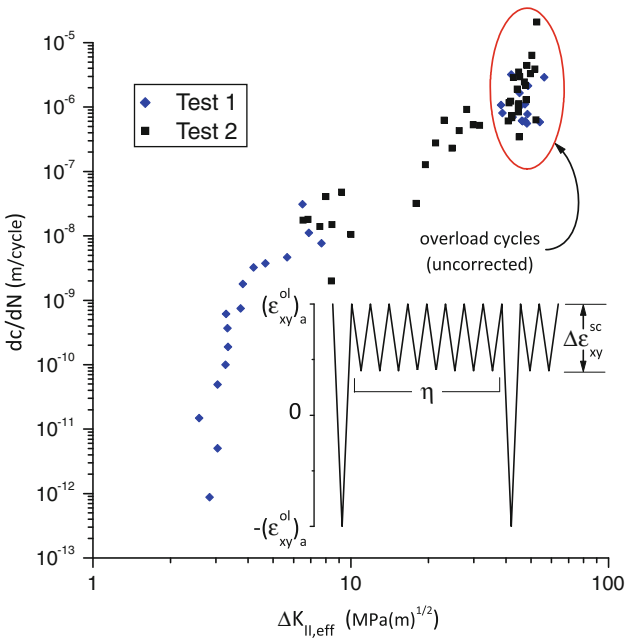

Fig. 17 Mode II crack face interference-free long crack growth data [5]

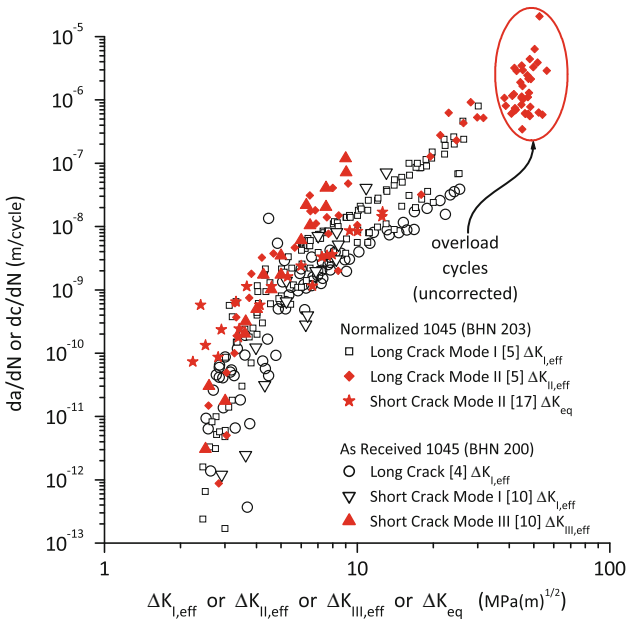

Fig. 18 Mode I, mode II, and mode III effective crack growth rate data for soft SAE 1045 steels combined [5]

the figure were applied often enough that the fatigue crack grew without crack face interference.

Mode II crack growth data obtained from these tests are shown on logarithmic axes of crack growth rate versus effective (crack face interference-free) strain intensity factor in Fig. 17. It is replotted together with mode I and mode III crack growth data from Fig. 17 in Fig. 18. It is clear that the data for all the three crack growth modes fall into a single band.

Estimates of the maximum shear crack length before changing over to crack growth on a tensile plane provided by the strain energy release rate and maximum crack growth rate models are shown together with experimental data from crack face interference-free torsion tests in Fig. 19. The data come from tests in a tension torsion test machine [5] on the specimen shown in Fig. 16 using the load history shown in the inset of Fig. 17 to induce crack face interference-free conditions. The material was an SAE 1045 steel in a normalized condition [5]. Above a crack length of 50 μm, the limit of resolution of the optical microscope used in the measurements, each of the two growth mode transition models describes a boundary with an increasing transition crack length as the strain amplitude increases terminating in an effective strain amplitude shown in the figure above which there will be no transition and cracks will grow to failure in shear. Most of the data show a change from a shear mode to a tensile mode growth at strain amplitudes and lengths greater than the crack growth rate model but less than the strain energy release rate model. There were a number of tests, which are circled in black in Fig. 19, in which cracks switched back to shear

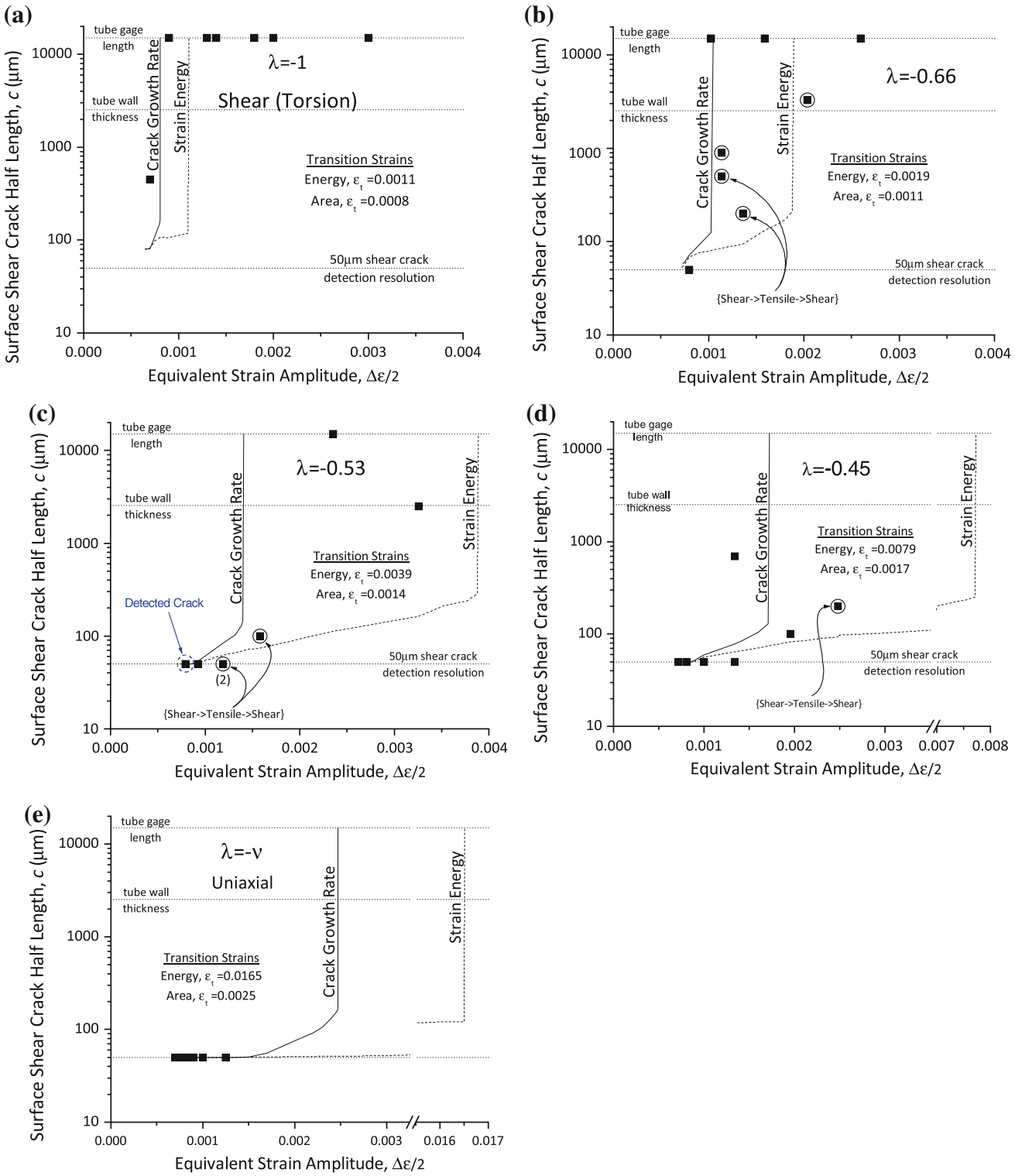

Fig. 19 Experimental observations and predictions of maximum shear crack lengths (before crack growth changes to maximum tensile planes). Data points with *black circles* indicate experiments in which, after the initial switch from growth in shear to growth on a tensile plane, the crack returned to growth on a shear plane. The shear crack length at the point of the initial switch to tensile plane growth is reported. For strains which exceed the transition strain, models predict a continuous shear crack that spans the gage length ($2c = 30$ mm) [5]

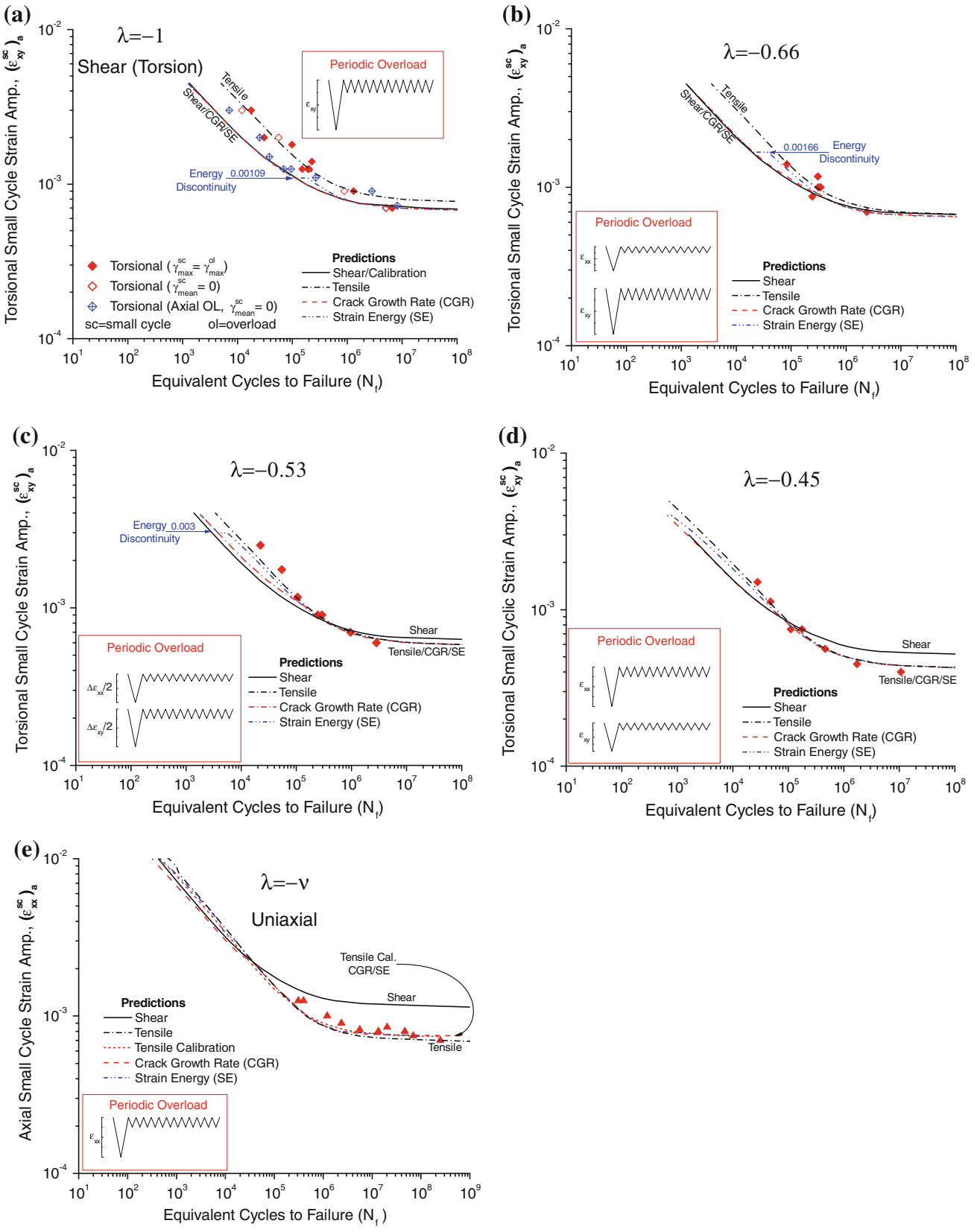

Fig. 20 Life predictions made with the Crack Growth Rate (CGR), Strain Energy (SE), shear and tensile models [5]

mode growth after changing to tensile mode growth, and in a few cases there were several switches back and forth.

Fatigue life predictions made using the strain energy release rate and crack growth rate crack length prediction models are shown together with crack face interference-free fatigue test data in Fig. 20. Also shown in the figure are "tensile" and "shear" predictions made assuming that all the crack growth took place in a tensile and a shear mode, respectively. The equivalent strain-life data have been adjusted to remove the crack growth due the overload cycles [5]. The mode change models give curves that fall close to each other and yield slightly conservative fatigue life estimates. The shear predictions are good (and close to the two mode change model predictions) for $\lambda = -1$ pure shear fatigue data and the tensile predictions are good (and close to the mode change models) for uniaxial fatigue data but both give progressively poorer predictions as the strain ratio moves toward the mode for which the other is good. The closeness of the fatigue life predictions of the two mode change prediction models and the shifting back and forth between modes is evidence of almost equal tensile and shear mode crack growth rates.

Conclusions

At low strain levels crack growth in uniaxial and equibiaxial strain ratios initiated in mode I shear on a maximum shear strain plane, and after traversing one or two grains, changed to mode I tensile growth normal to the maximum strain range axes for the rest of a test. The aspect ratio of the crack increased from an initial value near zero until it reached a ratio of about 0.8, and then maintained this shape until failure.

At strain ratios of -1 and -0.625 many cracks initiated at 40°–45° to the specimen axis and grew into the specimen in a shear mode while the aspect ratio of the crack increased from near zero to about 1 at 90% of the fatigue life. Failure then occurred by a rapid linking up of the microcracks.

The insertion of compressive overloads greatly increased crack growth rates and drastically reduced the fatigue life but did not change the crack shape development.

Uniaxial constant amplitude straining at a level near the fatigue limit resulted for the two notch geometries in a single crack that after reaching an approximately semicircular shape grew in mode I in the length and depth direction and maintained the semicircular shape until failure. At a constant amplitude strain level twice the fatigue limit, multiple cracks initiated and continuously linked up to maintain a very shallow crack shape that persisted until failure. At a strain level equal to 1.5 times the fatigue limit, a slower linking up of cracks maintained a crack shape midway between the above shapes. Similar changes in crack geometry with strain level were observed for the Grapple Skidder load history.

Special experimental techniques were developed to determine the crack face interference-free mode II crack growth rate data, and these curves fell into a single band with mode II and mode III short crack data.

Two crack growth models were used to predict both the maximum length of shear cracks observed in smooth tubes tested under in-phase biaxial loading and the crack face interference-free fatigue life—these models followed the growth of a crack from a shallow but long crack of persistent slip-band depth out to the failure crack length of $2c = 30$ mm.

Both models qualitatively predicted the maximum shear crack length trends: increased strain ratio and/or increased small cycle strain amplitudes led to longer maximum shear crack lengths.

Both models satisfactorily predicted the fatigue life of the smooth tubes for the biaxial strain ratios examined in this study ($\lambda = \varepsilon_{22}/\varepsilon_{11} = -1, -0.66, -0.53, -0.45$, and $-\nu$): neither predicted the life data substantially better than the other, and they both provided better predictions across the range of strain ratios than models in which all the crack growth was assumed to be confined to either the planes of maximum shear or planes of maximum tension.

References

1. Varvani-Farahani A, Topper TH (1999) In: Fatigue and fracture mechanics: 30th volume, ASTM STP 1360. American Society for Testing and Materials, Philadelphia, p 299
2. Varvani-Farahani A, Topper TH (1997) Int J Fatigue 19(7):589
3. Dabayeh AA, Topper TH (1995) Int J Fatigue 17(4):261
4. MacDougall C, Topper HT (1997) Int J Fatigue 19(5):389
5. Bonnen JJF, Topper TH (2008) Eng Fract Mech 75(3–4):804
6. Brown MW, Miller KJ (1973) Proc Inst Mech Eng 187(65):745
7. Socie D (1993) In: McDowell DL, Ellis R (eds) Advances in multiaxial fatigue. ASTM STP 1191. American Society for Testing and Materials (ASTM), Philadelphia, p 7
8. Varvani-Farahani A, Topper TH (1997) In: Nontraditional methods of sensing stress, strain, and damage in materials and structures, ASTM STP 1318. American Society for Testing and Materials, Philadelphia, p 43
9. Newman JC Jr, Edwards PR (1988) Short crack growth behaviour in an aluminum alloy—an AGARD cooperative test program. Technical report AGARD-R-732. AGARD, Paris
10. Varvani-Farahani A, Topper TH (2000) In: Newman JC, Piascik RS (eds) Fatigue crack growth thresholds, endurance limits, and design. ASTM STP 1372. American Society for Testing and Materials, West Conshohocken, p 192
11. Varvani-Farahani A, Topper TH, Plumtree A (1996) Fatigue Fract Eng Mater Struct 19(9):1153
12. Khalil ML (2002) Effect of fatigue loading on crack opening stress and crack shape development. PhD thesis, University of Waterloo, Waterloo

13. Abdel-Raouf H, Topper TH, Plumtree A (1992) Fatigue Fract Eng Mater Struct 15(9):895
14. Conle FA, Bonnen JJF (1999) In: Cordes T, Lease K (eds) Multiaxial fatigue of an induction hardened shaft, AE-28, Chap 3. Society of Automotive Engineers, Warrendale, p 23
15. Nuismer RJ (1975) Int J Fract 11:245
16. Hourlier F, Pineau A (1982) In: Francois D (ed) Advances in fracture research fracture 81, vol 4. Pergamon Press, Oxford, p 1833. Held in Cannes, March 29–April 3, 1981
17. Socie DF, Hua CT, Worthem DW (1987) Fatigue Fract Eng Mater Struct 10(1):1